[Osokogwn, 1(3): May., 2012]
ISSN: 2277-9655

IJESRT

INTERNATIONAL JOURNAL OF ENGINEERING SCIENCES & RESEARCH TECHNOLOGY

Computerized Modeling of Paraffin Wax Deposition in Inclined Multiphase Tubular System

Osokogwu, u.[1] and otung, d. A.[2]

Department of Petroleum Engineering, University of Port-Harcourt, Port-Harcourt, Nigeria

oxgoodlt@yahoo.com

Abstract

In recent times, the high demand for fossil fuel-derived energy is gradually moving the frontiers of oil exploration and production from conventional areas (such as land/shallow offshore) into more challenging locations. This trend has made issues associated with flow assurance in the oil and gas industry to become increasingly important. This is especially true of paraffin wax precipitation and subsequent deposition in areas of reduced temperatures, such the Polar Regions as well as deep sea environments. Therefore, in order to preclude or reduce costly remedial operations aimed at removing pipe/tubing blockages resulting from wax deposition, it is essential to be able to predict when, where, how and how much paraffin wax is deposited during the working life of oilfield installations. This knowledge will prove indispensable when the design and maintenance of oilfield equipment is to be undertaken. Thus, this work is concerned with the development of a computer model capable of making the necessary wax phase precipitation and deposition calculations in a multiphase environment. To make wax precipitation and deposition predictions in diverse flow conditions, use is made of EOS mathematical modeling (for making phase equilibrium calculations), energy and material balances as well as multi-phase pressure gradient correlations for the inclined tubular.

Keywords: Wax Deposition, Multiphase, Paraffin, Wax, Mathematical Modeling

Introduction

According to Schmidt (2010), the term "paraffin wax" simply refers to saturated hydrocarbons that contain more than 16 carbon atoms in the paraffin series ($C_{16} - C_{40}$) and are in solid state at room temperature. Paraffin's or alkenes are the homologous chemical family of saturated hydrocarbons that result from combining CH_2 groups in succession to form straight-chained molecules. Paraffin's could be either *n-paraffin's (straight chain), iso-paraffin's (branched) or cyclo- paraffin's (aromatic).* However, Becker (1997) maintains that straight-chain hydrocarbons constitute the bulk of crude oil mixtures (roughly 80-90% by composition).

Thus, paraffin waxes could be defined more generally as long-chained alkanes belonging to the homologous paraffin series that precipitate out of supersaturated crude-oil mixtures on cooling.

Apart from the fact that paraffin waxes form an important stock chemical for the petro-chemical industry, the study of paraffin is pertinent to us because of the inherent flow assurance issues associated with their precipitation and subsequent deposition.

Flow assurance is a production objective which seeks to ensure optimal flow rates at all foreseeable conditions in all production tubular/equipment conveying produced fluids beginning at the reservoir-well-bore interface to the treatment/refinery facility. The four (4) areas of focus in industrial oil production flow assurance include waxing (paraffinic deposition), asphaltenes deposition, sand ingress, and hydrate formation; these conditions tend to foul/block off production equipment during normal hydrocarbon production or transportation.

While the relative importance of other types of flow assurance issues is not by any means to be underestimated, this paper will focus only on the problem of wax precipitation and deposition in an oilfield tubular.

The formation of wax deposits in the transport of paraffinic oils presents several problems not limited to the reduction of the effective diameter of pipes, which in turn leads to additional pumping energy costs, and subsequent equipment failure.

The process of wax formation is triggered when the temperature of the crude falls to the Wax Appearance Temperature (WAT or Cloud Point Temperature). At this point, paraffin waxes begin to crystallize, thus entrapping the oil in a gel structure and forming deposits on the pipeline walls.

Since problems associated with wax deposition can prove to have high economic implications, an understanding of the mechanisms of the wax deposition (and subsequent modeling of these mechanisms) is likely to be a key step towards an optimum design, prevention and/or solution of the problem.

Literature Review

Perhaps, Svendsen (1993) was the first to develop a mathematical model for prediction of wax deposition in both open and closed pipeline systems by using a combination of analytical and numerical models.

From then on to 1996, thermodynamic wax precipitation models were assumed to be based on the regular-solution theory of mixtures, such that the precipitates from liquid/vapor hydrocarbon mixtures formed a solid solution. These solutions were either assumed to be ideal or non-ideal depending on the solution techniques to be employed. The non-idealities of the solution formed could be estimated using suitable activity coefficient models [see Coutinho et al. (1995) for an evaluation of these models]. Some authors that assumed the solid-solution model in wax precipitation calculations include Won (1986), Won (1989), Hansen et al. (1988), K. S. Pedersen et al. (1991), Pederson (1993), and Erickson et al. (1993).

Later on, Lira-Galeana et al. (1996) introduced the multi-solid model to describe the thermodynamic equilibrium of wax precipitation. In this model, the authors posited that wax precipitation in multi-component oil systems produces a solid mass that contains *mutually immiscible* precipitating components. The multi-solid model was independently corroborated by experimental studies of W. B. Pedersen et al. (1991) and of Snyder et al. (1992).

In 2008, Banki et al. (2008) applied the enthalpy-porosity model to explain wax deposition phenomena in an isothermal horizontal pipeline transporting crude oil. Banki et al. successfully used this approach to model the aging process of the wax deposit/gel layer.

The following are salient points that are immediately evident from the review of current literature:

- Previous studies done on wax deposition analysis are mostly restricted to laminar two-phase (i.e. zero water content and zero gas rate) flow in circular horizontal conduits. This limitation can readily be rationalized by the fact that such studies were mainly geared towards explaining waxing effects in pipeline systems where such conditions as two-phase flow (only liquid-oil phase and solid-wax phase are present) and laminar horizontal flow in circular pipes are to be expected. However, these conditions can quickly become inadequate when wax deposition prediction is to be undertaken in deviated production tubings, flow-lines and pipelines laid-up in hilly terrains. Thus, since features like inclined tubings, turbulence, and presence of gaseous and immiscible phases are encountered in real-life oilfield operations, it becomes imperative to incorporate these conditions into the original wax precipitation models.
- Due to the inherent difficulty of accounting for these field conditions using a 100% theoretical/mechanistic technique, this work will attempt to account for these conditions by taking a semi-empirical approach instead.

Scope of Work

Most of the previous studies carried out on the problem of predicting wax deposition in oil installations tended to be more or less limited in their scope of applicability such that stringent conditions of system configuration and boundary conditions have to be in effect before such models could effectively predict wax related phenomenon. However, in this work we will attempt to model wax deposition in the broadest possible sense such that most conditions regularly encountered in both upstream and downstream oil production could be readily accounted for.

In any case, certain simplifying assumptions still have to be made in order to facilitate the solution of the problem at hand. Thus, the following gives some of the more general assumptions that will form the basis of this work:

- Four distinct phases are accounted for in all calculations. These phases include: water-rich phase, oil phase, gaseous phase and solid phase (wax crystallites).
- The oil and gas phases are composed predominantly of n-alkanes (composition contributions from naphthenes and aromatics are ignored).
- The oil and water phases are considered immiscible.
- Water vapor content in the gaseous phase is considered negligible.
- Hydrate formation effects are not considered.
- Ambient thermo-properties (such as temperature, thermal gradients and heat conductivities or coefficients) are considered to be time-independent (i.e. non-transient).
- Asphaltenes deposition is not taken into account.

Model Development

The major objective of this work was to build a robust computer application capable of predicting wax precipitation and deposition along oilfield installations under various conditions of flow. Thus, a flow computational program named "WD-Predictor" has been designed and developed. The following procedure was followed:

i. The domain scope of the problem statement was clearly defined.
ii. Then mathematical models that approximate the physical behavior of wax crystallization and deposition systems were developed or reviewed. Pertinent models considered include:
   a. *Property Transport Models (Energy, Momentum and Mass)*
   b. *Thermodynamic Equilibrium Model*
   c. *Wax Deposition & Erosion Model*
iii. The mathematical models developed in (ii) above were discretized, approximated and/or solved directly
iv. Numerical solutions to the discretized models were then developed using appropriate algorithms and pseudo-codes.
v. A *computational flow dynamics* (**CFD**) program – WD-Predictor – implementing the developed models in (iii) and (iv) above as well as the accompanying user-interface was coded in C++ language.
vi. Finally, comprehensive model testing/verification (including stability analysis), code debugging and optimization was undergone to ensure that the models used are indeed representative of what is obtained in reality.

We consider a 3-Dimensional pipe/tubular network containing pipes of arbitrary diameters, lengths and deviations. Such a network could be approximated by finite straight sections of inclined pipe segments of variable lengths (***Δl***). Segments are chosen such that along the segment length, pipe properties (such as thermal and dimensions) do not change and pipe-fittings are not encountered. Thus, a pipe segment will have a constant internal diameter (***d***), a length (***L***) an inclination (***θ***) and an overall heat transfer coefficient (***U***) – fig 1.

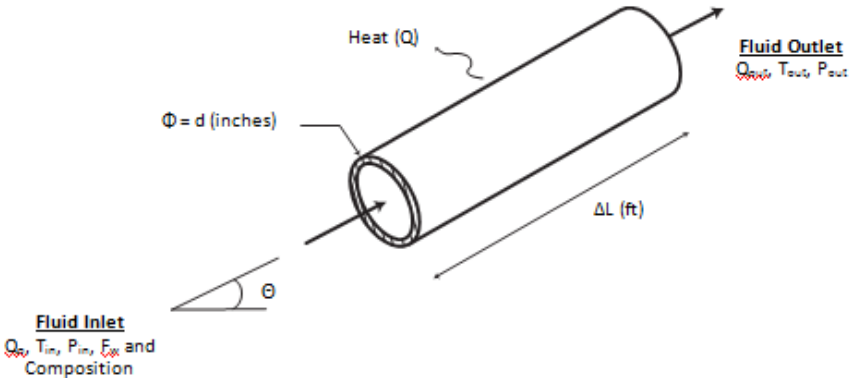

Figure 1: Straight Pipe Segment Approximation

Nichita D. et al. (2001) and *Heidemann R. A. et al.* (2005) maintain that the multi-solid model can describe the **WAT** and the amount of precipitation more accurately than the solid solution model. Hence, in this work we will make use of the multi-solid model by *Lira-Galeana et al.* (1996). Here, each precipitated component forms a solid layer, which does not mix with the other solid layers.

The vapor-liquid equilibrium will be established by the Peng-Robinson (1976) Equation of State which gives a suitable description of the fugacity coefficients for hydrocarbons.

The multi-solid wax precipitation model involves carrying a solid-liquid phase stability analysis prior to solving appropriate component material balances. The phase stability criterion is expressed as:

$$f_{Li}(P,T,z) - f_{S\,(pure\,i)}(P,T) \geq 0, \quad i \sim 1,2,\dots,n \tag{1}$$

The liquid fugacity can be described by the PR-EOS while the solid-state fugacity for each component could be approximated by the equation (6) in Lira-Galeana et al.

The material balances for both precipitating and non-precipitating components are shown in the following equations. For non-precipitating components:

$$z_i F - x_i[F - S - V] - y_i V = 0, \quad i \sim 1,2,\dots,N - N_p \tag{2}$$

For precipitating components:

$$z_i F - x_i[F - S - V] - s_i S - y_i V = 0, \quad i \sim (N - N_p + 1),\dots,N \tag{3}$$

With the following constraints,

$$\sum_{i=1}^{N} z_i = \sum_{i=1}^{N} x_i = \sum_{i=1}^{N} y_i = \sum_{i=1}^{N} s_i = 1 \tag{4}$$

$$F = L + V + S \tag{5}$$

$$y_i = K_i x_i \tag{6}$$

The vapor-liquid-solid equilibrium calculation involves finding the solutions to equations (2) and (3). The vapor-liquid thermodynamic equilibrium for all components is directly implied by equation (6); thus to satisfy the liquid-solid equilibrium, the following expressions must be incorporated into equation (3) for the precipitating components:

$$x_i = \frac{f_{S\,pure\,i}(P,T)}{\varphi_{Li} P}, \quad i = (N - N_p + 1),\dots,N \tag{7}$$

$$y_i = \frac{f_{S\,pure\,i}(P,T)}{\varphi_{Vi} P}, \quad i = (N - N_p + 1),\dots,N \tag{8}$$

Using (6) to make x_i and y_i subject of formula in equation (3) yields the following equations for the non-precipitating components:

$$x_i = \frac{z_i}{1 - S/F + (K_i - 1)V/F}, \quad i \sim 1,2,\dots,N - N_p \tag{9}$$

$$y_i = \frac{K_i z_i}{1 - S/F + (K_i - 1)V/F}, \quad i \sim 1,2,\dots,N - N_p \tag{10}$$

By performing a summation of equations (9) and (10) over all non-precipitating components gives,

$$\sum_{i=1}^{N-N_p} x_i = \sum_{i=1}^{N-N_p} \frac{z_i}{1 - S/F + (K_i - 1)V/F} \tag{11}$$

$$\sum_{i=1}^{N-N_p} y_i = \sum_{i=1}^{N-N_p} \frac{K_i z_i}{1 - S/F + (K_i - 1)V/F} \tag{12}$$

Noting from equation (4) that,

$$\sum_{i=1}^{N} x_i = \sum_{i=1}^{N-N_p} x_i + \sum_{i=N-N_p+1}^{N} x_i = 1 \tag{13}$$

And,

$$\sum_{i=1}^{N} y_i = \sum_{i=1}^{N-N_p} y_i + \sum_{i=N-N_p+1}^{N} y_i = 1 \tag{14}$$

Then, equations (11) and (12) can be rewritten as,

$$\sum_{i=1}^{N-N_p} x_i = \sum_{i=1}^{N-N_p} \frac{z_i}{1 - S/F + (K_i - 1)V/F} = 1 - \left[\sum_{i=N-N_p+1}^{N} x_i\right] \tag{15}$$

$$\sum_{i=1}^{N-N_p} y_i = \sum_{i=1}^{N-N_p} \frac{K_i z_i}{1 - S/F + (K_i - 1)V/F} = 1 - \left[\sum_{i=N-N_p+1}^{N} y_i\right] \tag{16}$$

Re-arranging equations 15 and 16 gives,

$$\left[\sum_{i=1}^{N-N_p} \frac{z_i}{1 - S/F + (K_i - 1)V/F}\right] + \left[\sum_{i=N-N_p+1}^{N} x_i\right] - 1 = 0 \tag{17}$$

$$\left[\sum_{i=1}^{N-N_p} \frac{K_i z_i}{1 - S/F + (K_i - 1)V/F}\right] + \left[\sum_{i=N-N_p+1}^{N} y_i\right] - 1 = 0 \tag{18}$$

The second terms on the left side of equations (17) and (18) represent the summation of all precipitating component fractions in the liquid and gaseous phases respectively. Thus, the compositions in the equations above could be replaced by the precipitating component composition fractions given in equations (7) and (8).
Therefore,

$$\left[\sum_{i=1}^{N-N_p} \frac{z_i}{1 - S/F + (K_i - 1)V/F}\right] + \left[\sum_{i=N-N_p+1}^{N} \frac{f_{S\,pure\,i}(P,T)}{\varphi_{Li} P}\right] - 1 = 0 \tag{19}$$

$$\left[\sum_{i=1}^{N-N_p} \frac{K_i z_i}{1 - S/F + (K_i - 1)V/F}\right] + \left[\sum_{i=N-N_p+1}^{N} \frac{f_{S\,pure\,i}(P,T)}{\varphi_{Vi} P}\right] - 1 = 0 \tag{20}$$

Assuming fugacity coefficients and k-values are independent of fluid compositions; then, equations (19) and (20) represent 2 equations in 2 unknowns (*S/F* and *V/F*), which could be solved simultaneously. Due to the implicit nature of the equations being considered, an analytical solution of the system is almost impossible. Therefore, the equations have to be treated using an appropriate numerical scheme.

In this work, the Newton-Raphson iterative root-finding scheme for a system of non-linear equations was used. To facilitate the development of the N-R algorithm for the solution of the equations, *F* is arbitrarily set as 1 – so that *S* represents solid moles precipitated per feed mole and *V* represents number of moles in the gaseous phase per feed mole. Then,

$$G(S,V) = \left[\sum_{i=1}^{N-N_p} \frac{z_i}{1-S+(K_i-1)V}\right] + \left[\sum_{i=N-N_p+1}^{N} \frac{f_{S\,pure\,i}}{\varphi_{Li}P}\right] - 1 = 0 \tag{21}$$

$$H(S,V) = \left[\sum_{i=1}^{N-N_p} \frac{K_i z_i}{1-S+(K_i-1)V}\right] + \left[\sum_{i=N-N_p+1}^{N} \frac{f_{S\,pure\,i}}{\varphi_{Vi}P}\right] - 1 = 0 \tag{22}$$

The N-R algorithm consists of:

i. Making an initial guess of **S** and **V** (the Predictor step)
ii. Implementing the **NR** correction formula for the S and V parameters
iii. Ensuring the parameters **S** and **V** are constrained within physically conceivable limits
iv. Checking **S** and **V** parameters for convergence
v. Repeating the procedure from (ii) if convergence is not achieved.

It can be easily shown that the NR correction formula for ***S*** and ***V*** is given in matrix form as:

$$\frac{\partial(G,H)}{\partial(S,V)}\begin{pmatrix}\delta S\\ \delta V\end{pmatrix} = -\begin{pmatrix}G(S,V)\\ H(S,V)\end{pmatrix} \tag{23}$$

In the above equation, the first term is known as the Gaussian matrix and is given as,

$$\frac{\partial(G,H)}{\partial(S,V)} = \begin{pmatrix}\frac{\partial G}{\partial S} & \frac{\partial G}{\partial V}\\ \frac{\partial H}{\partial S} & \frac{\partial H}{\partial V}\end{pmatrix} \tag{24}$$

And the second term is the correction vector for the ***S*** and ***V*** parameters. The NR correction step is carried out by pre-multiplying the right-hand side of the equation (23) by the inverse of the Gaussian matrix. Thus, by defining the following,

$$\begin{aligned}
a &= \frac{\partial G}{\partial S} = \sum_{i=1}^{N-N_p} \frac{K_i z_i}{[1-S+(K_i-1)V]^2}\\
b &= \frac{\partial G}{\partial V} = \sum_{i=1}^{N-N_p} \frac{-z_i K_i (K_i-1)}{[1-S+(K_i-1)V]^2}\\
c &= \frac{\partial H}{\partial S} = \sum_{i=1}^{N-N_p} \frac{z_i}{[1-S+(K_i-1)V]^2}\\
d &= \frac{\partial H}{\partial V} = \sum_{i=1}^{N-N_p} \frac{-z_i (K_i-1)}{[1-S+(K_i-1)V]^2}
\end{aligned} \tag{25}$$

The Gaussian inverse could be written as:

$$\begin{pmatrix}\frac{\partial G}{\partial S} & \frac{\partial G}{\partial V}\\ \frac{\partial H}{\partial S} & \frac{\partial H}{\partial V}\end{pmatrix}^{-1} = \frac{1}{\left(\frac{\partial G}{\partial S}\cdot\frac{\partial H}{\partial V} - \frac{\partial G}{\partial V}\cdot\frac{\partial H}{\partial S}\right)} \times \begin{pmatrix}\frac{\partial H}{\partial V} & -\frac{\partial G}{\partial V}\\ -\frac{\partial H}{\partial S} & \frac{\partial G}{\partial S}\end{pmatrix} \tag{26}$$

Hence, the NR corrections for $\boldsymbol{V}$ and $\boldsymbol{S}$ are,

$$\boldsymbol{\delta S} = \frac{\boldsymbol{G}\cdot\frac{\boldsymbol{\partial H}}{\boldsymbol{\partial V}} - \boldsymbol{H}\cdot\frac{\boldsymbol{\partial G}}{\boldsymbol{\partial V}}}{\left(\frac{\boldsymbol{\partial G}}{\boldsymbol{\partial V}}\cdot\frac{\boldsymbol{\partial H}}{\boldsymbol{\partial S}}\right) - \left(\frac{\boldsymbol{\partial G}}{\boldsymbol{\partial S}}\cdot\frac{\boldsymbol{\partial H}}{\boldsymbol{\partial V}}\right)} \tag{27}$$

$$\boldsymbol{\delta V} = \frac{\boldsymbol{H}\cdot\frac{\boldsymbol{\partial G}}{\boldsymbol{\partial S}} - \boldsymbol{G}\cdot\frac{\boldsymbol{\partial H}}{\boldsymbol{\partial S}}}{\left(\frac{\boldsymbol{\partial G}}{\boldsymbol{\partial V}}\cdot\frac{\boldsymbol{\partial H}}{\boldsymbol{\partial S}}\right) - \left(\frac{\boldsymbol{\partial G}}{\boldsymbol{\partial S}}\cdot\frac{\boldsymbol{\partial H}}{\boldsymbol{\partial V}}\right)} \tag{28}$$

As noted earlier, the values of corrected $\boldsymbol{V}$ and $\boldsymbol{S}$ must be bounded to ensure physically plausible solutions are obtained. Therefore, the constraint equations for the solutions of $\boldsymbol{V}$ and $\boldsymbol{S}$ are:

$$\begin{aligned} \boldsymbol{S}^{m+1} &= \boldsymbol{S}^{m} + \delta\mathbf{S} \geq 0, \\ \boldsymbol{V}^{m+1} &= \boldsymbol{V}^{m} + \delta\mathbf{V} \geq 0, \end{aligned} \tag{29}$$

And,

$$\boldsymbol{S}^{m+1} + \boldsymbol{V}^{m+1} \leq 1$$

The NR iterations are terminated when the corrections for the solid and vapor mole fractions are smaller than a predetermined tolerance value. At this point, the V and S parameters give the corresponding equilibrium Vapor and Wax splits respectively. The Liquid split is gotten by subtracting the sum of V and S from unity.

The compositions of the precipitating components in the solid phase are gotten from equation (3) as:

$$\boldsymbol{s_i} = \frac{\boldsymbol{z_i} - \boldsymbol{x_i}[\mathbf{1} - \boldsymbol{S} - \boldsymbol{V}] - \boldsymbol{K_i x_i V}}{\boldsymbol{S}}, \qquad \boldsymbol{i} \sim \left(\boldsymbol{N} - \boldsymbol{N_p} + \mathbf{1}\right), \ldots, \boldsymbol{N} \tag{30}$$

The compositions of the precipitating components in the liquid and vapor phases are derived from equations (7) and (8) while that for the non-precipitating phase are calculated from (9) and (10) respectively.

Finally, it must be noted that as in the Vapor-Liquid Equilibria discussed the k-values are in fact not independent of composition. Hence, this procedure must be repeated over and over until compositions and/or split ratios converge.

The conservation of mass simply means that for a given control volume such as a segment of pipe, the mass in minus the mass out must equal the mass accumulation within the segment. Then, for a constant-area duct,

$$\frac{\boldsymbol{\partial \rho}}{\boldsymbol{\partial t}} + \frac{\boldsymbol{\partial(\rho v)}}{\boldsymbol{\partial L}} = \mathbf{0} \tag{31}$$

For steady-state flow, no mass accumulation can occur and the equation above then becomes:

$$\frac{\boldsymbol{\partial(\rho v)}}{\boldsymbol{\partial L}} = \mathbf{0} \tag{32}$$

The above mass balance equation is simply known as the continuity equation. Application of Newton's first law to fluid flow in pipes requires that the rate of momentum out, minus the rate of momentum in, plus the rate of momentum accumulation in a given pipe segment must equal the sum of all forces on the fluids.

Conservation of linear momentum can be expressed as:

$$\frac{\boldsymbol{\partial(\rho v)}}{\boldsymbol{\partial t}} + \frac{\boldsymbol{\partial(\rho v^2)}}{\boldsymbol{\partial L}} = -\frac{\boldsymbol{\partial P}}{\boldsymbol{\partial L}} - \boldsymbol{\tau}\frac{\boldsymbol{\pi d}}{\boldsymbol{A}} - \boldsymbol{\rho g}\sin\boldsymbol{\theta} \tag{33}$$

Combining the equation above with the continuity equation and assuming steady-state flow gives:

$$\frac{\boldsymbol{\partial P}}{\boldsymbol{\partial L}} = -\boldsymbol{\tau}\frac{\boldsymbol{\pi d}}{\boldsymbol{A}} - \boldsymbol{\rho g}\sin\boldsymbol{\theta} - \boldsymbol{\rho v}\frac{\boldsymbol{\partial v}}{\boldsymbol{\partial t}} \tag{34}$$

The equation above is frequently called the mechanical energy balance equation. The mechanical energy balance equation clearly shows that the steady-state pressure gradient along a pipe is made up of three components (see equation 35). Thus, the mass and momentum conservation equations together form the pressure distribution equation for a pipe segment.

$$\left(\frac{\boldsymbol{\partial P}}{\boldsymbol{\partial L}}\right)_{\boldsymbol{T}} = \left(\frac{\boldsymbol{\partial P}}{\boldsymbol{\partial L}}\right)_{\boldsymbol{friction}} + \left(\frac{\boldsymbol{\partial P}}{\boldsymbol{\partial L}}\right)_{\boldsymbol{elev}} + \left(\frac{\boldsymbol{\partial P}}{\boldsymbol{\partial L}}\right)_{\boldsymbol{accel}} \tag{35}$$

For simple pipe and flow conditions (such as laminar single-phase flow in a horizontal pipeline) it is possible to solve equation (34) analytically to yield the pressure distribution field within the pipe segment. However, in typical field conditions, situations arise where multi-phase flow and other non-ideal conditions (such as turbulent and inclined-pipe flow) make it impossible to solve equation (34) without resorting to empirical techniques.

In this work, equation 34 will be approximated by the Beggs and Brill (1973) multi-phase flow pressure prediction procedure. The choice of the Beggs and Brill procedure was necessitated by the following features of the correlation:

- The correlation directly corrects for inclination of pipe segments
- The correlation accounts for different flow patterns
- Due consideration is given to gas slippage

The Beggs and Brill (1973) correlation for the total pressure gradient is given generally as:

$$\left(\frac{\partial P}{\partial L}\right)_T = \frac{\frac{f\rho_n v_m^2}{2d} + \rho_s g \sin\theta}{1 - E_K} \tag{36}$$

The monograph by Brill and Murkherjee (1999) provides in-depth details on the equation shown above. The general procedure for the Beggs and Brill multiphase correlation is as follows:

i. Flow Pattern prediction
ii. Liquid Hold-up prediction
iii. Liquid Hold-up correction for inclination
iv. Friction Factor prediction
v. Pressure Gradient calculation

The Payne et al. (1979) modification to the Beggs and Brill correlation was also used in this work.

Application of energy conservation to fluid flow in pipes requires that in a given pipe segment the energy in, minus the energy out, plus the heat transferred to or from the surroundings must equal the rate of energy accumulation.

$$\frac{\partial\langle\rho e\rangle}{\partial t} = -\frac{\partial}{\partial L}\left[\rho v\left(e + \frac{P}{\rho g_c J}\right)\right] - \frac{Q\pi d}{A} \tag{37}$$

The parameter, J is the mechanical equivalent of heat and is necessary when dealing with customary units where mechanical energy and thermal energy have different units (in field units J is approximately **777.86** lbf - ft/BTU).

$$\frac{\partial\langle\rho e\rangle}{\partial t} + \frac{Q\pi d}{A} = -\rho v\frac{\partial}{\partial L}\left(e + \frac{P}{\rho g_c J}\right) - \left(e + \frac{P}{\rho g_c J}\right)\cdot\frac{\partial\langle\rho v\rangle}{\partial L} \tag{38}$$

In the equations above, e is the intrinsic specific energy and is defined by

$$e = \frac{gLsin\theta}{g_c J} + \frac{v^2}{2g_c J} + u \tag{39}$$

Therefore, by incorporating the continuity equation and equation (39) into equation (38) and assuming average fluid density varies only slightly with time, equation 38 yields

$$\rho\frac{\partial}{\partial t}\left(\frac{gLsin\theta}{g_c J} + \frac{v^2}{2g_c J} + u\right) + \frac{Q\pi d}{A} = -\rho v\frac{\partial}{\partial L}\left(\frac{gLsin\theta}{g_c J} + \frac{v^2}{2g_c J} + u + \frac{P}{\rho g_c J}\right) \tag{40}$$

Since the inclination of the pipe segment is assumed time independent, the first term on the left-hand side of the equation 40 vanishes. In addition, by ignoring the change in kinetic energy of the fluid in the pipe segment with time, equation 40 can be rewritten as,

$$\rho\frac{\partial u}{\partial t} + \frac{Q\pi d}{A} = -\rho v\frac{\partial}{\partial L}\left(\frac{gLsin\theta}{g_c J} + \frac{v^2}{2g_c J} + u + \frac{P}{\rho g_c J}\right) \tag{41}$$

Because specific enthalpy is defined as

$$h = u + \frac{P}{\rho g_c J} \tag{42}$$

Equation 41 can be expressed as

$$\rho\frac{\partial u}{\partial t}+\frac{Q\pi d}{A}=-\rho v\frac{gsin\theta}{g_cJ}-\rho v\frac{\partial h}{\partial L}-\frac{\rho v^2}{g_cJ}\frac{\partial v}{\partial L} \quad (43)$$

$$\frac{1}{v}\cdot\frac{\partial u}{\partial t}+\frac{Q\pi d}{w}=-\frac{gsin\theta}{g_cJ}-\frac{\partial h}{\partial L}-\frac{v}{g_cJ}\frac{\partial v}{\partial L} \quad (44)$$

The heat flux to the surroundings, Q is defined in terms of the overall heat-transfer coefficient, U and temperature difference between the fluids and the surroundings. Thus,

$$Q=U[T-T_a] \quad (45)$$

Where,

$$T_a=T_{ai}-g_GLsin\theta$$

Secondly, it can be readily shown that assuming small phase-change effects along the pipe segment, the enthalpy gradient is given by

$$\frac{\partial h}{\partial L}=C_P\frac{\partial T}{\partial L}-C_P\eta\frac{\partial P}{\partial L} \quad (46)$$

Where η represents the Joule-Thomson coefficient and represents isenthalpic cooling (or heating) by expansion. Also, the internal energy change with time (if fusion and vaporization heats are neglected) can be approximated by the following formulation in constant volume specific heat capacity,

$$\left(\frac{\partial u}{\partial t}\right)_V=C_V\left(\frac{\partial T}{\partial t}\right)_V \quad (47)$$

Finally, by assuming that the change in fluid velocity across the pipe segment is insignificant, then equation 44 can be expressed as

$$\frac{C_V}{v}\cdot\frac{\partial T}{\partial t}+\frac{U\pi d[T-T_{ai}+g_GLsin\theta]}{w}=-\frac{gsin\theta}{g_cJ}-C_P\frac{\partial T}{\partial L}+C_P\eta\frac{\partial P}{\partial L} \quad (48)$$

The above equation can be discretized using the backward difference numerical scheme to yield the numerical solution for the average temperature of the pipe segment at any time level (n+1) as,

$$T_{av}^{n+1}=\frac{H}{\left(\frac{C_P}{L}+\frac{U\pi d}{2w}+\frac{C_V}{v\Delta t}\right)} \quad (49)$$

Where,

$$H=-C_P\left(\frac{T_{av}^n-T_{in}^n-T_{in}^{n+1}}{L}\right)+C_P\eta\frac{\partial P}{\partial L}-\frac{gsin\theta}{g_cJ}-\frac{U\pi d}{w}\times\left(\frac{T_{av}^n}{2}-T_{ai}+g_G\frac{Lsin\theta}{2}\right)+\frac{C_V}{v}\cdot\left(\frac{T_{av}^n}{\Delta t}\right)$$

At time level zero (0) (i.e. at initial flow conditions), the temperature profile can be described by the numerical scheme,

$$T_{av}^0=T_{in}^0+\frac{L}{2C_P}\times\left(C_P\eta\frac{\partial P}{\partial L}-\frac{gsin\theta}{g_cJ}\right) \quad (50)$$

After the precipitation of wax within an oil field installation (such as a pipeline or production tubing), the final deposition of the wax crystals on the pipe/tubing wall depends on a number of factors including amount of wax precipitated, gross fluid rate, temperature gradient across the fluid segment, pipe wall roughness and turbulence effect. The deposition of wax on tubular walls will necessarily require the transport of the crystals from the main fluid stream to the wall bounds through various transport phenomena including *molecular diffusion*, *shear dispersion*, *Brownian diffusion* and *gravity settling*.

Apart from transport phenomena that carry wax crystals to the pipe walls, erosion of wax deposits from pipe walls due to high fluid rates (sometimes carrying along abrasive solids) also influence the variation of wax thickness with time on pipes surfaces. In order to accurately model the deposition of wax along pipe segments, the fraction of precipitated wax that eventually makes it to the pipe must be estimated.

Let the fraction of the precipitated wax phase that actually gets deposited on a unit length of pipe wall be given as **φ**. Then the solid wax phase exiting the pipe segment and consequently entering the subsequent pipe segment will be given as **(1 – φ)**. Continuing in the same reasoning, the fraction of wax exiting the second segment is:

$$(\mathbf{1} - \quad)(\mathbf{1} - \quad) = (\mathbf{1} - \quad)^{\mathbf{2}} \tag{51}$$

Carrying on in this fashion, if the pipe is (L) units in length, then the fraction of wax entering it that exits un-deposited is $\mathbf{(1-\varphi)}^{\mathbf{L}}$ and that deposited is, $\mathbf{1-(1-\varphi)}^{\mathbf{L}}$.

The nature of the function **φ** has to be determined empirically such that the effects of various deposition phenomena are factored in. Thus, a suitable form of **φ** can be expressed as:

$$= \boldsymbol{A}\left(\frac{\boldsymbol{\epsilon}}{\boldsymbol{d}}\right) \times \left[\frac{\mathbf{1}}{\mathbf{1} + \boldsymbol{B}\left(\frac{\boldsymbol{\mu w}}{\boldsymbol{\rho \pi d^3}}\right)}\right] \times \left[\mathbf{1} - \frac{\boldsymbol{T_a}}{\boldsymbol{T}}\right]^{\boldsymbol{C}} \tag{51}$$

Where A, B, and C are empirically determined constants

The first term on the right hand side represents the relative pipe roughness. Typically, with larger pipe roughness values the tendency for wax crystals to stick to the tubing walls becomes more pronounced. The second term is a representation of the turbulence rate of the flow – and it reflects the impact of wax erosion due to high fluid flow rates or turbulence. The last term is a dimensionless temperature ratio (i.e. ambient temperature to fluid temperature) to factor in the effect of temperature gradient – and hence diffusion – on wax crystal transport.

In summary, a generalized solution approach is described below:

Break the pipe/tubing network into discrete pipe segments – the smaller the pipe segments the better the accuracy of the results generated. Define $\mathbf{P_{in}}$ = Inlet Feed Pressure; $\mathbf{T_{in}}$ = Inlet Feed Temperature; and **Composition** = Inlet Feed Composition.

1. Given $\mathbf{T_{in}}$, $\mathbf{P_{in}}$ and Inlet **Composition**, guess $\mathbf{P_{out}}$ and $\mathbf{T_{out}}$. If no other information is available let $\mathbf{P_{out}} = \mathbf{P_{in}}$ and $\mathbf{T_{out}} = \mathbf{T_{in}}$.
2. Perform a thermodynamic equilibrium calculation of the feed at $\mathbf{P_{av}} = (\mathbf{P_{in}} + \mathbf{P_{out}})/2$ and $\mathbf{T_{av}} = (\mathbf{T_{in}} + \mathbf{T_{out}})/2$
3. Calculate all necessary correlation parameters at $\mathbf{P_{av}}$ and $\mathbf{T_{av}}$
4. Estimate the pressure gradient **dP**/**dL** and hence $\mathbf{P^*_{out}}$ using the Beggs and Brill correlation
5. Evaluate all thermo-physical properties at $\mathbf{P_{av}}$ and $\mathbf{T_{av}}$
6. Estimate $\mathbf{T^*_{av}}$ and hence $\mathbf{T^*_{out}}$ using the energy balance equation
7. Compare $\mathbf{P^*_{out}}$ and $\mathbf{T^*_{out}}$ to $\mathbf{P_{out}}$ and $\mathbf{T_{out}}$ respectively. If they are outside a specified tolerance range then set $\mathbf{P_{out}} = \mathbf{P^*_{out}}$ and $\mathbf{T_{out}} = \mathbf{P^*_{out}}$ and jump to 3
8. The amount of wax deposited in the current pipe segment and in the current time step is given as the wax precipitation rate from the previous time step multiplied by the time step. Deposited wax composition can likewise be updated by simply using material balance calculations.
9. Jump to 2 (until all the pipe segments have been analyzed). For step 2, use $\mathbf{P_{in}} = \mathbf{P_{out}}$ from previous pipe segment; $\mathbf{T_{in}} = \mathbf{T_{out}}$ from previous pipe segment; and Inlet **Composition** = Feed composition into previous pipe segment less wax deposited in previous pipe segment
10. Jump to 2 (until the calculation time period has been reached). Set $\mathbf{P_{in}}$ = Feed inlet pressure; $\mathbf{T_{in}}$ = Feed Inlet Temperature; Inlet **Composition** = Feed Composition; and Current Pipe segment = Inlet segment.
11. The solution is thus presented as wax deposited (thickness and composition) in each pipe segment (location) per time step

The wax precipitation and deposition model discussed thus far should provide a reasonable enough accuracy when the time steps and pipe segment lengths are chosen to be relatively small. However, there are limits beyond which reducing the time step and segment lengths will not result in improved accuracy. These limits are brought about mainly by the inherent inaccuracies introduced into the model by empirical modeling. Generally, the wax precipitation/deposition model developed will rely heavily on correlations for fluid properties at different conditions of pressure and temperature. These correlations sometimes can prove to be unreliable, thus introducing serious errors into model solutions. In addition, some of the simplifying assumptions introduced into the model to ensure that a tractable solution is arrived at could lead to severe restrictions on the achievable accuracy. Some of such assumptions include:

- Neglecting the presence of water vapor in the gaseous phase
- Ignoring the slight but considerable solubility of:
  - the gaseous phase in the aqueous phase
  - the oil phase in the aqueous phase
  - water in the oil phase
- Assuming a time-independent overall heat transfer coefficient
- Assuming that the kinetic energy of the fluids flowing through a constant diameter tubular is both position and time independent

Results and Discussion

This section presents the results obtained by the application of the computer program discussed to the prediction of waxing-related phenomena oil production and transport. Here, the wax prediction model is used to estimate the Wax Appearance Temperature (WAT) or Cloud Point Temperature (CPT) of three crude samples. These estimates will be compared to experimental results as published in the literature. The subsequent sub-section will compare the steady-state pressure and temperature outputs as functions of position from the wax-deposition-predictor program, WD-Predictor, with that obtained from a popular commercial pipe simulator such as PROSPER™. Next, an illustration on how well the wax-thickness ratio computed by WD-Predictor compares with experimental data extracted from Cordoba and Schall (2001). Finally, we will compare the WD-Predictor output on wax deposit thickness with that generated with the enthalpy-porosity model proposed by Banki et al. (2008).

• Cloud-Point Temperature Prediction

WD-Predictor contains a dedicated module for the prediction of the WAT of oil samples at any given pressure. The program was tested on 3 different oil samples gotten from literature. The sample composition properties (the molar weights, critical pressures, critical temperatures, critical volumes, acentric factors and mole percentages) are presented in Table 1.

Table 1: Oil Sample Properties

						OIL NUMBER		
						I	II	III
COMPONENT	**WEIGHT**	**T_{ci} (F)**	**P_{ci} (psia)**	**V_{ci} (cft/lb)**	**ω**	*Mol %*	*Mol %*	*Mol %*
C1	16.0429	-116.4118	673.0736	1.5858	0.0115	*1.1390*	*0.0000*	*0.2457*
C2	30.0699	90.1004	708.3424	2.3707	0.0986	*0.5070*	*0.0041*	*0.3433*
C3	44.0970	206.1464	617.3762	3.2037	0.1524	*0.4810*	*0.0375*	*1.2781*
C4	58.1240	305.6882	550.6530	4.0845	0.2010	*0.6340*	*0.0752*	*2.3328*
i-C4	58.1240	274.9028	529.0424	4.2129	0.1848	*0.5630*	*0.1245*	*0.8048*
C5	72.1510	385.6100	489.5197	4.9816	0.2539	*0.5150*	*0.3270*	*2.2744*
i-C5	72.1510	369.0464	483.4962	4.9335	0.2222	*1.1130*	*0.2831*	*1.8304*
C6	86.1779	454.5464	439.6992	5.8948	0.3007	*2.0030*	*0.3637*	*4.3526*
C7	100.2050	512.6144	396.9363	6.8235	0.3498	*5.4780*	*3.2913*	*7.0409*

C8	114.2320	563.8064	362.1040	7.7850	0.4018	*8.7560*	*8.2920*	*8.5073*
C9	128.2590	610.6064	333.5969	8.6979	0.4455	*7.2220*	*10.6557*	*6.2413*
C10	142.2850	652.0064	305.6742	9.6426	0.4885	*5.4140*	*11.3986*	*5.9502*
C11	156.3130	689.2682	284.9889	10.5722	0.5350	*5.3230*	*10.1595*	*4.7261*
C12	170.3390	725.2682	265.4074	11.4207	0.5620	*4.5710*	*8.7254*	*4.1475*
C13	184.3670	756.7682	249.9768	12.4942	0.6230	*5.2890*	*8.5434*	*4.2760*
C14	198.3800	789.5300	234.9872	13.2952	0.6790	*4.7200*	*6.7661*	*3.5380*
C15	212.4100	812.9300	219.9946	14.0959	0.7060	*4.4450*	*5.4968*	*4.0267*
C16	226.4290	830.9300	206.0348	15.0569	0.7650	*3.5590*	*3.5481*	*3.0915*
C17	240.4570	860.3960	191.0002	16.1115	0.7700	*3.6420*	*3.2366*	*2.7944*
C18	254.4790	881.7980	175.9989	17.1398	0.8000	*3.1040*	*2.1652*	*2.8950*
C19	268.5100	901.0022	161.9999	18.1009	0.8270	*2.7170*	*1.8098*	*2.6891*
C20	282.5400	922.7300	168.2437	19.0620	0.9069	*2.5970*	*1.4525*	*2.2190*
C21	296.5830	940.7300	160.9918	19.9393	0.9420	*1.9360*	*1.2406*	*2.0459*
C22	310.5880	956.9300	153.7400	20.8421	0.9722	*2.0390*	*1.1081*	*1.9448*
C23	324.6090	973.1300	147.9385	21.7217	1.0262	*1.6610*	*0.9890*	*1.7398*
C24	338.6390	987.5300	142.1369	22.6040	1.0710	*1.6160*	*0.7886*	*1.6283*
C25	352.6700	1001.9300	137.7858	23.4627	1.1053	*1.4210*	*0.7625*	*1.4660*
C26	366.6900	1014.5300	131.9843	24.3194	1.1544	*1.2330*	*0.6506*	*1.2924*
C27	380.7200	1027.1300	128.0683	25.1602	1.2136	*1.4260*	*0.5625*	*1.1907*
C28	394.7390	1037.9300	123.2820	25.9858	1.2375	*1.3430*	*0.5203*	*1.1033*
C29	408.7690	1048.7300	119.8011	26.7998	1.2653	*1.3000*	*0.4891*	*0.9935*
C30+	422.7990	1093.7300	125.8927	27.6083	1.3072	*13.2300*	*6.1326*	*10.9902*

The composition of oil sample 1 was gotten from Lira-Galeana et al. (1996) while oil samples 2 and 3 where extracted from Pan et al. (1997). Table 2 shows both predicted and experimental CPTs of the three oil samples.

Table 2: Predicted WATs

Oil Sample	Exp. WAT (°F)	Model (°F)	Error (°F)
OIL 1	87.800	89.888	2.08
OIL 2	114.35	115.76	1.41
OIL 3	72.950	70.620	-2.33

As can be seen in Table 2, the predicted Wax Appearance Temperatures agree quite well with the values obtained experimentally. It should be noted that the WATs in the table were all measured/calculated at standard atmospheric pressure (14.7 psia).

- **Pressure and Temperature Profiles**

In order to validate the models used for predicting the pressure and temperature fields (i.e. the momentum and thermal energy balance equations), the output of the WD-Predictor was compared to the output from the program PROSPER™ developed by the Petroleum Experts Group.

PROSPER™ is a popular pipe simulation package that has gained wide acceptance in the industry. Thus, the results reported by the program will most likely be free of programmatic bugs – since due to its widespread patronage such programming errors would have been removed in subsequent updates/versions of the application. Thus, by

comparing the pressure and temperature distributions from the program designed in this work to the well-tested PROSPER™ we could quickly point out inconsistencies in the WD-Predictor program.

Table 3: Input Data for Analysis in Section 5.2

PARAMETER	VALUE
Pipe Length	5200 ft
Inclination	90^o (Vertical)
Diameter	5.5 inches
Composition	Oil Sample 2
P_{inlet}	4360 psia
T_{inlet}	250^oF
$T_{ambient}$	60^oF
Geothermal Gradient	$2.0^oF/100$ ft
Q_{oil}	1000 STB/d
Water Cut (f_w)	0.0
Duration	N/A (Steady-State)

The temperature and pressure fields compared were generated at steady-state condition using the input data specified in Table 3. The resulting profiles were plotted in figures 2 and 3 for the temperature and pressure fields respectively. The charts show how the temperature and pressure vary with depth in a vertical producing oil well. The predictions by PROSPER™ (using the Beggs and Brill correlation for Tubing Performance Relationship) in both charts are close to those by our program; hence, for the flow conditions given, it is safe to say that the WD-Predictor reports consistent results.

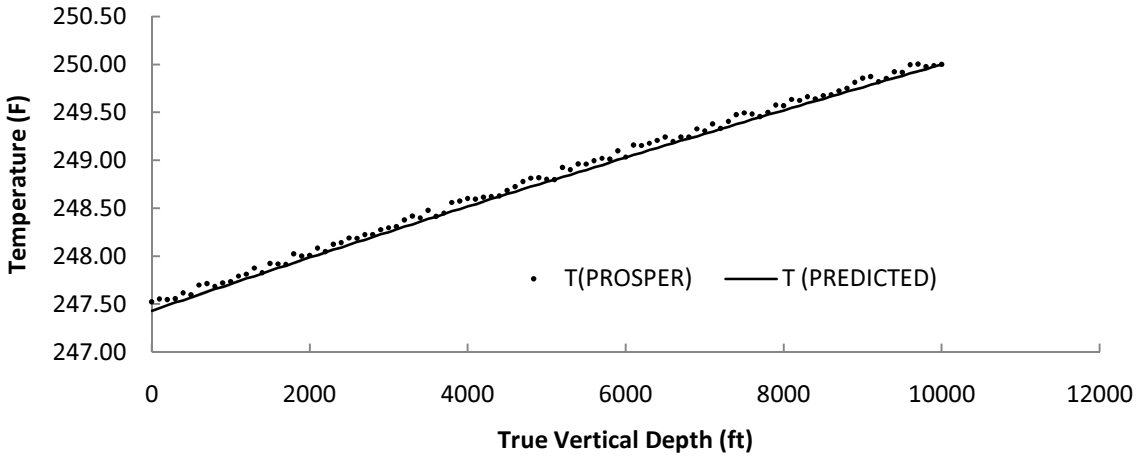

Figure 2: Temperature Profile Comparison

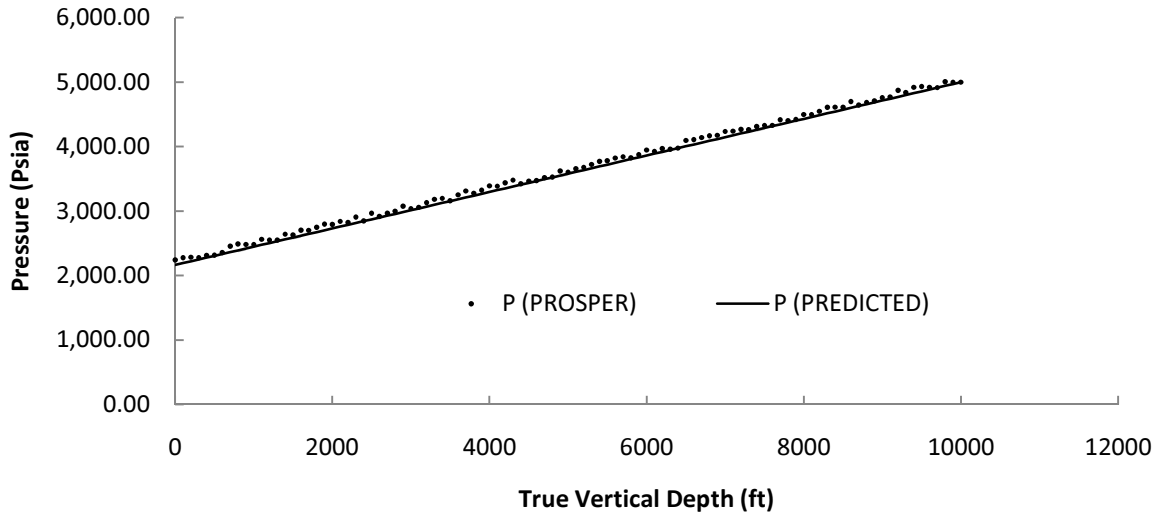

Figure 3: Pressure Field Comparison

- **Wax Deposition Thickness Ratio**

In this example, the wax thickness predictions from WD-Predictor are compared with the experimental data by Cordoba and Schall (2001). These authors measured the wax deposition thickness in a flow loop system. The fluid mixture consisted of a light oil species (n-octane) and a heavy cyclo-alkane (nonadecyl-cyclohexane: $CycloC_6C_{19}$). Wax formation was investigated as a function of time in a 25.4cm testing tube. The flow conditions and other relevant data are presented in Table 4.

The wax deposition thickness ratio is given by δ/R (where δ is the average wax deposit thickness, and R is the pipe inner radius). Figure (4) shows that the predictions from WD-Predictor and the measured data (three datasets) show good agreement.

Table 4: Input Data for Analysis in Section 5.3. Adapted from Cordoba and Schall (2001)

PARAMETER	VALUE
Pipe Length	0.8333 ft
Inclination	0^o (Horizontal)
Diameter	0.14496 inches
Z_{nC8}	0.67
$Z_{cycloC6\text{-}C19}$	0.33
T_{inlet}	77^oF
$T_{ambient}$	32^oF
Overall HTC (U)	50.928 BTU/hr-ft^2-^oF
Q_{oil}	0.5714 STB/d
Duration	120 minutes

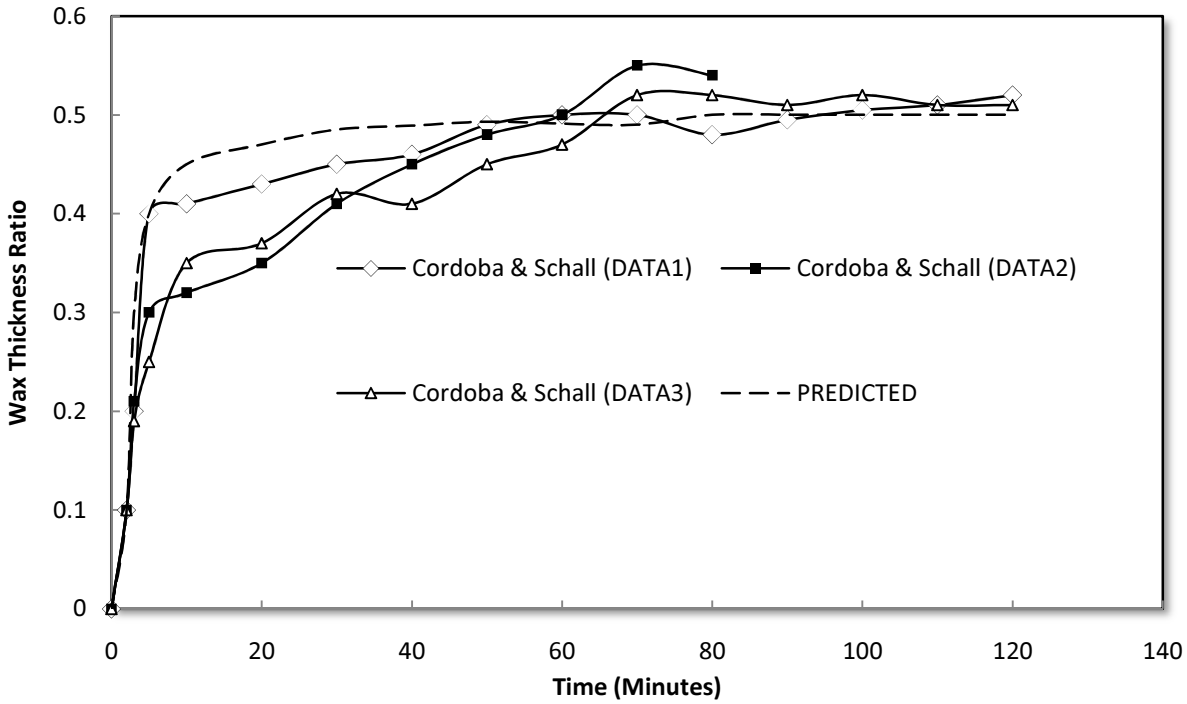

Figure 4: Wax Thickness Ratio (Measured and Predicted)

- **Comparison with the Enthalpy-Porosity Model**

Currently, the enthalpy-porosity model is the thermodynamic model that best accounts for waxing phenomena in oil piping systems. However, as has been noted in previously, the model suffers from restrictions in system configuration, such that inclined pipe and multi-phase flow conditions cannot be readily modeled.

Table 5 provides relevant input data to be used to compare the outputs of the enthalpy-porosity approach with that of the WD-Predictor program. The figures 5 and 6 show that there is a good agreement with the model proposed by Banki et al. (2008).

Table 5: Input Data for Analysis in Section 5.4

PARAMETER	VALUE
Pipe Length	3280 ft
Inclination	0^o (Horizontal)
Diameter	11.8 inches
Z_{nC8}	0.67
$Z_{cycloC6-C19}$	0.33
T_{inlet}	102^oF
$T_{ambient}$	75^oF
Overall HTC (U)	90.48 BTU/hr-ft^2-^oF
Q_{oil}	82.35 STB/d
Duration	1 Year

[Osokogwn, 1(3): May., 2012]
ISSN: 2277-9655

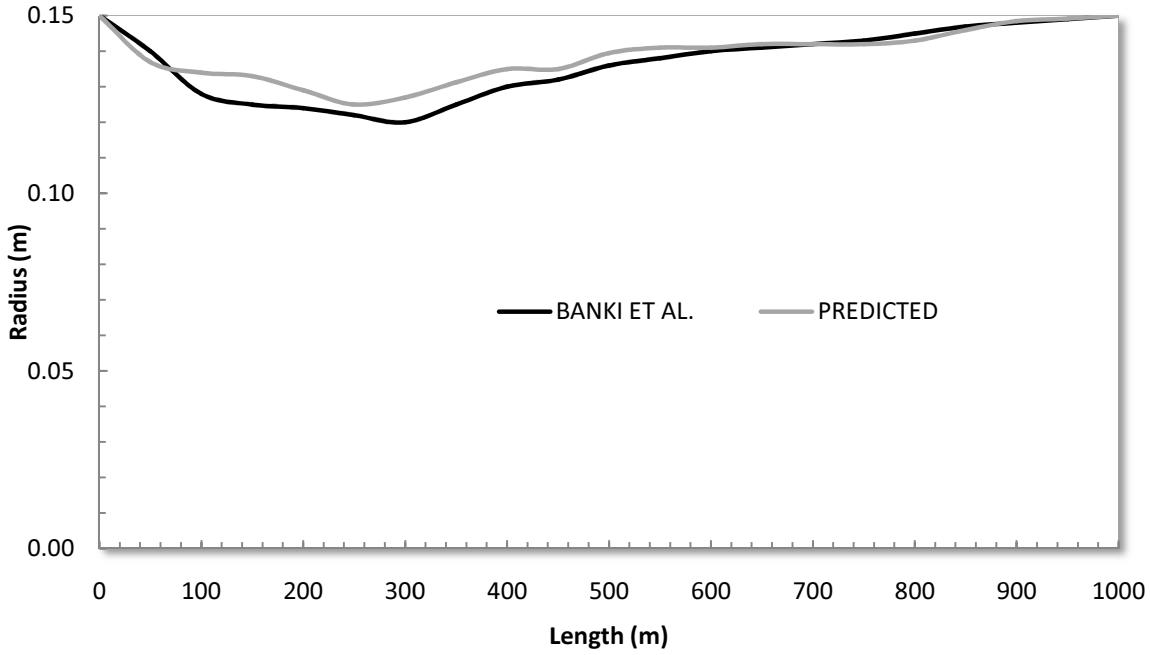

Figure 5: Pipe Radii at 5 months

However, the output from the WD-Predictor systematically predicts that the wax thickness is smaller than that from the enthalpy-porosity model. The reason for this discrepancy can be explained by the fact that our model does not take into due consideration the formation of a gel layer between the main fluid stream and the wax surface. This gel layer allows fluid to flow through – both radial and axial – and generally hardens/ages with time (due to the diffusion of wax forming molecules from the fluid stream into the gel region).

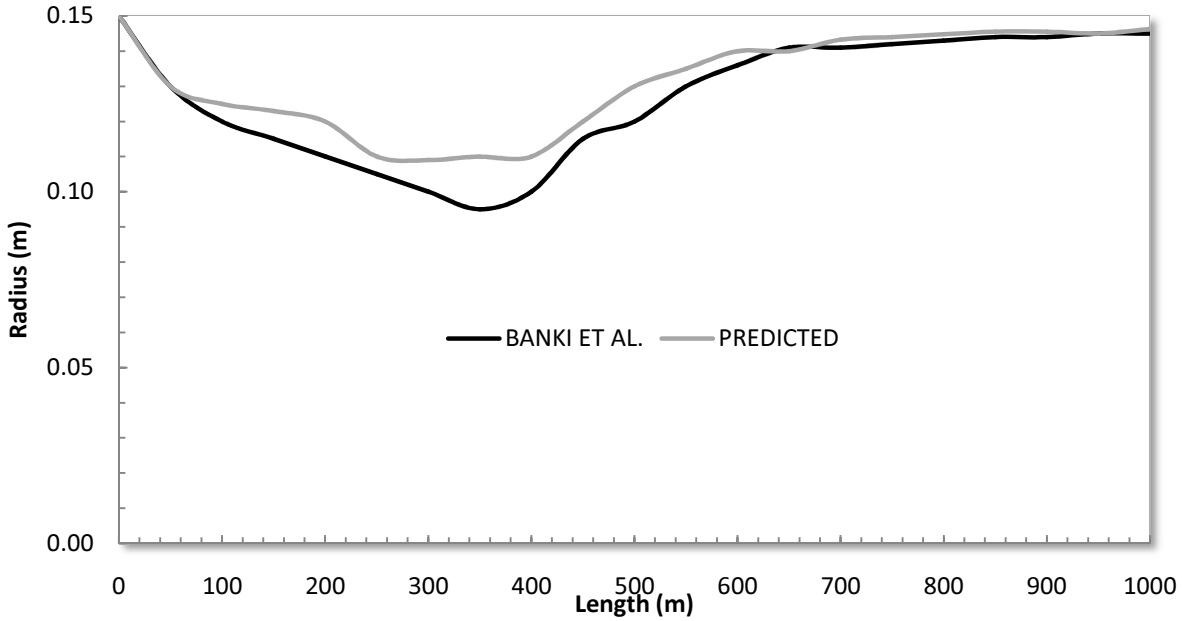

Figure 6: Pipe Radii after 1 year

Conclusion

In summary, this work was concerned with the creation of a computer program that will function as a high-end paraffin wax prediction tool. This application was designed to account for most conditions occurring in oil and gas production facilities during transport of well effluents from the reservoir to the consumer. Such conditions include flow through inclined pipes/tubular, multi-phase effects (such as gas slippage and flow patterns) as well as presence of a separate water-rich phase.

The methodology adapted to realize the design of the program (known as WD-Predictor) included the specification of a domain and subsequent application of relevant physical laws (with their accompanying mathematical models such as the transport and equilibrium models) to the domain. After converting the mathematical expressions into appropriate numerical equations, the program was coded in C++ and compiled for the x86 Windows™ platform.

The program as well as all underlying models were tested and verified with data sourced from appropriate literature. Program outputs such as oil sample CPTs, pressure and temperature fields as well as wax location and thicknesses were used to verify the models used. Analyses of the aforementioned outputs indicate that the program, WD-Predictor indeed should find relevance in the oil and gas business.

The following are recommendations made to ardent researchers intent on furthering the concepts developed in this work to create a full-blown wax analysis software,

- To ensure greater accuracy in phase equilibrium calculations, the water phase should be incorporated into VLE calculations.
- Better results could be obtained from the energy balance equation by employing a transient (time-dependent) overall heat transfer coefficient.
- At low temperature – high pressure production conditions, the formation of hydrates, especially in light-weight hydrocarbon fluid streams becomes highly probable. Thus, not accounting for hydrate formation effects could lead to serious errors in wax deposition calculations.
- Likewise, asphaltene deposition prediction should be concomitantly carried out with the paraffin deposition calculations.
- The effect of Naphthenes and Aromatic species as wells as other impurities like Nitrogen, Hydrogen Sulfide, Carbon IV Oxide and Oxygen should be accounted for.
- The influence of sand carrying effluent on the deposition and erosion or otherwise of wax crystals should also be modeled.
- Model deposition on pipe fittings and accessories should be included.
- Finally, the computer simulator should be upgraded to model down-stream pipelining (transport) of waxy crude using the enthalpy-porosity approach as suggested by Banki (2008).

Nomenclature

P = Pressure (psia)
T = Temperature (^{o}F)
F = Number of feed moles
S = Total number of moles precipitated
V = Total number of moles in the vapor phase
L = Total number of moles in the liquid phase
$\mathbf{s_i}$ = Mole fraction of component (i) in the solid phase
$\mathbf{x_i}$ = Mole fraction of component (i) in the liquid phase
$\mathbf{y_i}$ = Mole fraction of component (i) in the vapor phase
$\mathbf{K_i}$ = Vapor-liquid equilibrium constant for component (i)
$\mathbf{z_i}$ = Mole fraction of component (i) in the feed
n = Number of components
N = Number of components

N_P = Number of Precipitating components
f_L = Liquid Fugacity
f_S = Solid Fugacity
φ = Fugacity Coefficient
S^m = m^{th} Solution of the solid fraction
V^m = m^{th} Solution of the vapor fraction
T_{av}^n = Average temperature of a pipe segment at time level n
C_p = Constant pressure specific heat capacity
C_v = Constant volume specific heat capacity
L = Length of pipe segment
U = Overall heat transfer coefficient
w = Mass rate flow
ρ = Density
v = In-situ fluid velocity
Δt = Fixed time step
T_{in}^n = Average temperature at pipe inlet at time level n
η = Joule-Thomson coefficient
g_c = 32.2 lbf/lbm-ft s^{-2}
θ = Pipe segment inclination angle
g_G = Thermal gradient
T_{ai} = Ambient temperature at pipe segment inlet
ϵ/d = Pipe relative roughness

References

1. **Banki R., Hoteit H. and Firoozabadi A. (2008):** "*Mathematical Formulation and numerical modeling of wax deposition in pipelines from enthalpy-porosity approach and irreversible thermodynamics*", International Journal of heat and Mass Transfer.
2. **Becker J. R. (1997):** "*Crude oil waxes, emulsions and asphaltenes*", Tulsa, OK, USA: Penn Well Publishing Company.
3. **Beggs H. D. and Brill J.P. (1973):** "*A Study of Two-Phase Flow in Inclined Pipes*," JPT 607, Trans., AIME, pg. 255
4. **Brill J. P. and Mukherjee H. (1999):** "*Multiphase flow in wells*," Henry L. Doherty Memorial Fund of AIME, SPE.
5. **Burger E.D., Perkins T.K., Striegler J.H. (1981):** "Studies *of Wax Deposition in the Trans-Alaska Pipeline*", JPT.
6. **Chukwuma F. O. (2007):** "*The Theory and Design of Separation Processes*", M&J Grand Orbit Communications, pp 125.
7. **Cordoba A. J., Schall C. A. (2001):** "*Solvent migration in a paraffin deposits*" Fuel 80, pp 1279–1284
8. **Coutinho J.A.P., Simon I. A., Erling H. S. (1995):** "*Evaluation of activity coefficient models in prediction of alkane solid-liquid equilibria*", Fluid Phase Equilibria Vol. 103, pp 23 – 39.
9. **Erickson D.D., Niesen V.G., and Brown T.S. (1993):** "*Thermodynamic Measurements and Prediction of Paraffin Precipitation in Crude Oil*", SPE 26604, 68th Annual Technical Conference and Exhibition — Houston, Texas.
10. **Firoozabadi A., (1999):** "*Thermodynamics of Hydrocarbon Reservoirs*", McGraw-Hill, New York.
11. **Hansen J. H., Fredenslund A., Pedersen K. S., and Ronningsen H. P. (1988):** "*A Thermodynamic Model for Predicting Wax Formation in Crude Oils*," AIChE J., Vol. 34(12), pp 1937.

12. **Lira-Galeana C., Firoozabadi A., and Prausnitz J. M. (1996):** *"Thermodynamics of Wax Precipitation in Petroleum Mixtures"*, AIChE Journal, January 1996, Vol. 42, No. 1, pp 239–248.
13. **Nichita D., Goua L. l., Firoozabadi A. (2001):** *"Wax precipitation in gas condensate systems"*, SPE Prod. Facility, Vol. 16 (4), pp 250–259.
14. **Pan H., Firoozabadi A., and Fotland P. (1997):** *"Pressure and Composition Effect on Wax Precipitation: Experimental Data and Model Results"*, SPE Production & Facilities, pp 250–258.
15. **Payne G. A. (1979):** *"Evaluation of Inclined-Pipe Two-Phase Liquid Holdup and Pressure-Loss Correlations using Experimental Data,"* JPT 1198; Trans., AIME.
16. **Pedersen K. S. (1993):** *"Prediction of Cloud-Point Temperatures and Amount of Wax Precipitation,"* paper SPE 27629, SPE, Richardson, TX.
17. Pedersen K. S., Skovborg P., and Ronningsen H. P. (1991): "*Wax Precipitation from North Sea Crude Oils–4: Thermodynamic Modeling"*, Energy & Fuels, Vol. 5, No. 6, pp 924–932.
18. **Pedersen W. B., Hansen A. B., Larsen E., Nielsen A. B., and Ronningsen H. P. (1991):** *"Wax Precipitation from North-Sea Crude Oils: 2. Solid-Phase Content as Function of Temperature Determined by Pulsed NMR,"* Energy and Fuels, Vol. 5, pp 908.
19. **Peng D.-Y., and Robinson D. B. (1976):** "*A New Two-Constant Equation of State*", Ind. Eng. Chem. Fund., Vol. 15, pp 59.
20. **Rachford H. H. and Rice J. D. (1952):** J. Pet. Tech., 4(10), Section 1, p 19, and Section 2, p 3.
21. **Schmidt L. (2010):** *"CBU technical training: paraffin wax and asphaltene fundamentals and paraffin wax treatment for oil wells"*, Calgary, AB, Canada: Champion Technologies PowerPoint presentation.
22. **Snyder, R. G., Conti G., Strauss H. L., and Dorset D. L. (1993):***"Thermally- Induced Mixing in Partially Microphase Segregated Binary n-Alkane Crystals,"* J. Phys. Chem. Vol. 97, 7342.
23. **Snyder, R. G., Goh M. C., Srivatsavoy V. J. P., Strauss H. L., and Dorset D. L. (1992):** *"Measurement of the Growth Kinetics of Microdomdins in Binary n-AIkane Solid Solutions by Infrared Spectroscopy,"* J . Physics and Chemistry, 96, 10008.
24. **Snyder, R. G., Srivatsavoy V. J. P., Cates D. A., Strauss H. L., White J. W., and Dorset D. L., (1994):** *"Hydrogen/Deuterium Isotope Effects on Micro-phase Separation in Unstable Crystalline Mixtures of Binary n-Alkanes,"* J. Phys. Chem., Vol. 98 pp 674.
25. **Soave, G. (1972):** *"Equilibrium Constants from a Modified Redlich-Kwong Equation of State,"* Chem. Eng. Sci. Vol. 27, pp 1197.
26. **Svendsen J.A. (1993):** *"Mathematical Modelling of Wax Deposition in Oil Pipeline Systems"* AIche Journal, August, 1993.
27. **Van Wingen, N. (1950):** "*Recovery of Oil in the United States*" API, New York City.
28. **Vulk M. and Sarica C. (2003):** *"Tulsa university paraffin project"*, Department of Petroleum Engineering. University of Tulsa, Tulsa, Oklahoma.
29. **Weingarten J.S. and Euchner J.A. (1986):** "*Methods for Predicting Wax Precipitation and Deposition"*, SPE 15654, 61st Annual Technical Conference and Exhibition — New Orleans, Louisiana.
30. **Won K. W. (1989):** *"Thermodynamic Calculation of Cloud Point Temperatures and Wax Phase Compositions of Refined Hydrocarbon Mixtures,"* Fluid Phase Equil., Vol. 53, pp 377.
31. **Won K.W. (1986):** *"Thermodynamics for Solid Solution-Liquid- Vapor Equilibria: Wax Phase Formation from Heavy Hydrocarbon Mixtures"*, Fluid Phase Equilibria, Vol. 30, pp 265–279.

Appendix

The following pictures are screenshots of the program "WD-Predictor" that depict different operations carried out in the analysis of paraffinic crude oil.

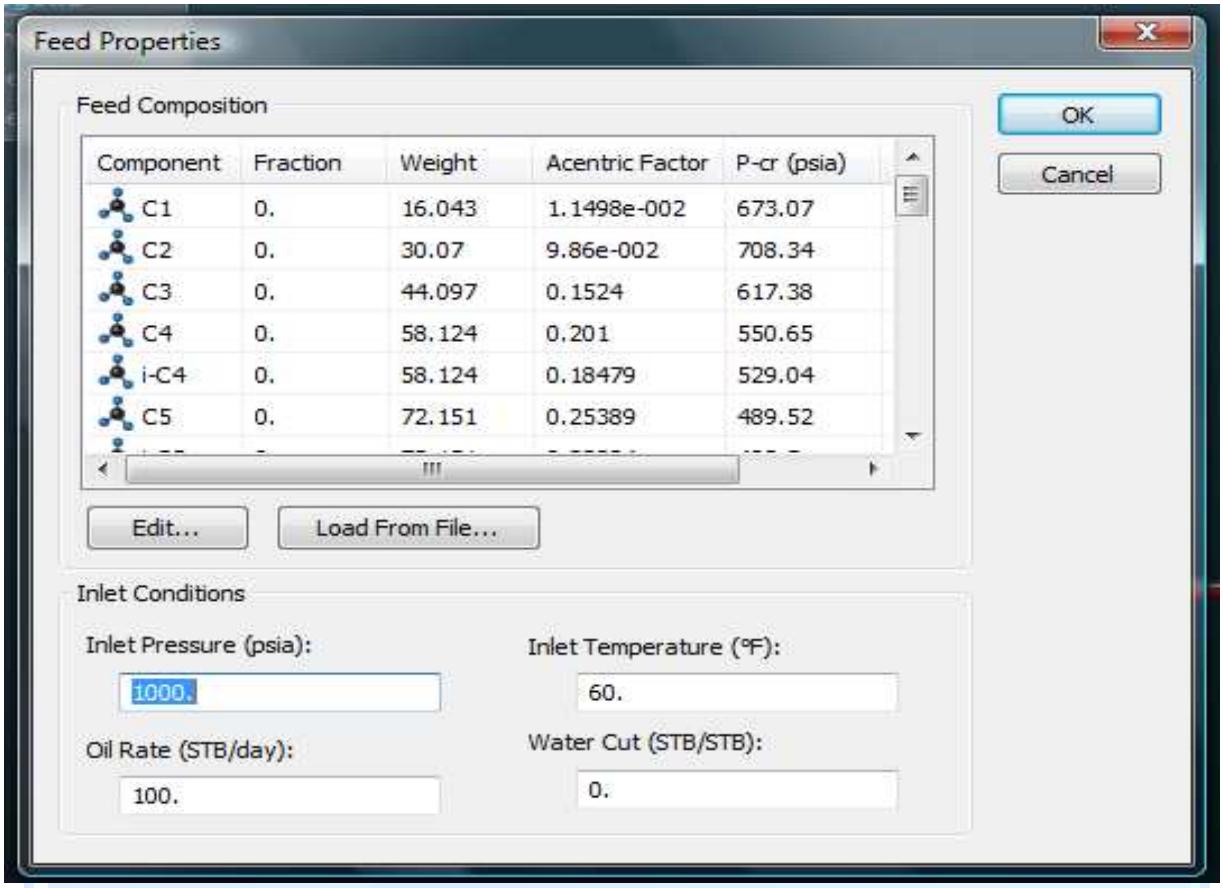

Figure A.1: Feed Properties Input Dialog

Figure A.1 above shows the program feed input system. Here, parameters like the feed composition fraction; weight; acentric factors and critical properties could be readily edited or loaded from an external file.

Other inlet conditions like the pressure and temperature at the inlet as well as water cut and oil flow rates are specified in the Feed Properties Dialog. The dialog is accessed by selecting general settings in the program ribbon and subsequently choosing “edit” in the Feed Properties group on the sidebar.
The next screenshot, figure A.2 shows a small applet embedded within WD-Predictor that specifically analyzes precipitation and vaporization properties of paraffinic crude samples. The types of analyses this applet can perform include the determination of:

- *Wax appearance temperature*
- *Cloud-Point pressure*
- *Bubble Point temperature and pressure*
- *Dew Point pressure and temperature*

It was with this sub-routine that the results in table 2 were generated.

[Osokogwn, 1(3): May., 2012]
ISSN: 2277-9655

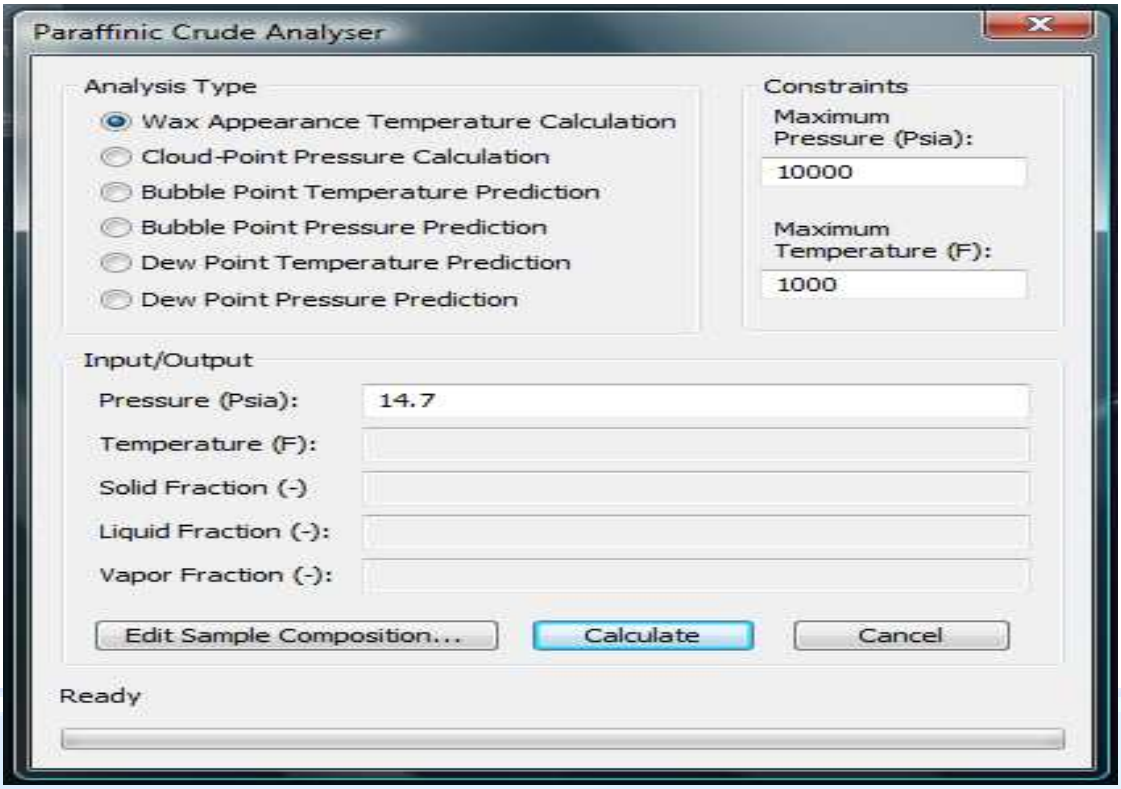

Figure A.2: Sub-routine for finding the WAT, WAP, Dew and Bubble Points of Crude Samples

Figure A.3 shows the progress dialog that pops up when the deposition analysis on pipe segments is initiated. It simply displays the current pipe segment being processed, and the time step and position at which the calculation is being done.

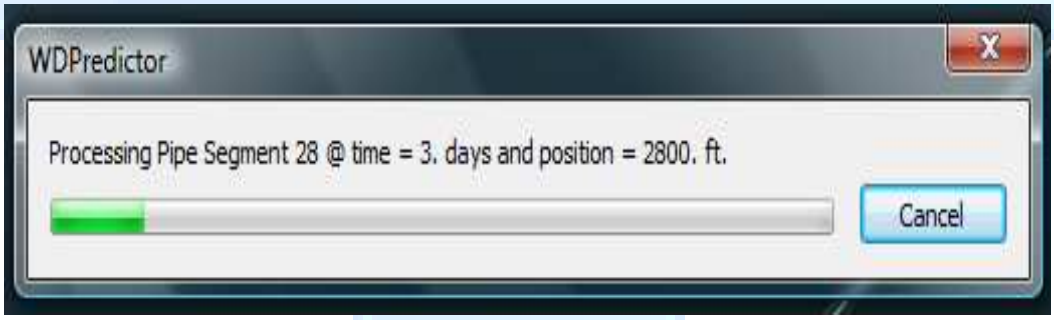

Figure A.3: WD-Predictor processing paraffin deposition in pipe segments

The final screenshot, figure A.4 shows the final program display after all calculations have been carried out. The outputted deposition result is usually displayed as a line graph that varies with both time and pipe position as shown.

[Osokogwn, 1(3): May., 2012]
ISSN: 2277-9655

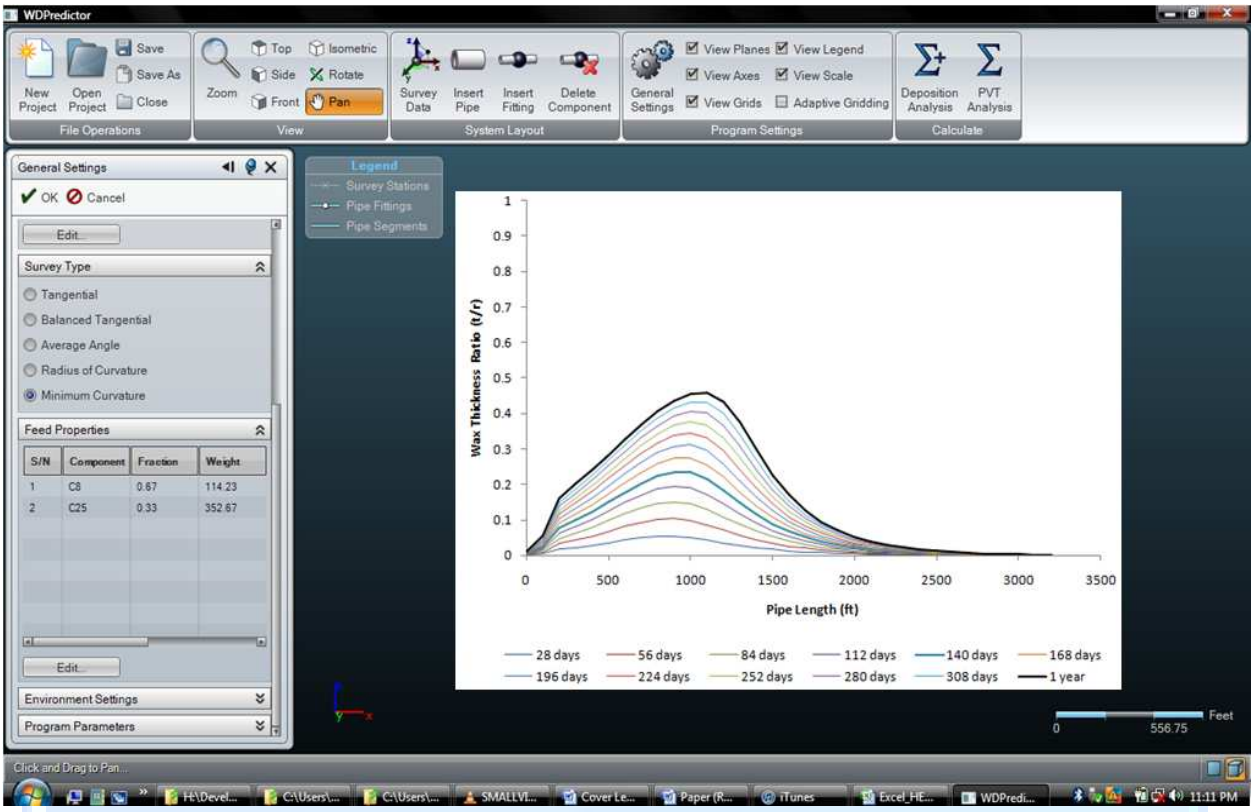

Figure A.4: WD-Predictor Environment showing displayed result

Table 6: Physical Properties of Wax Crystals

Alkane	Formula	Boiling point [°C]	Melting point [°C]	Density [g/cm3] (at 20°C)
Methane	CH_4	-162	-183	gas
Ethane	C_2H_6	-89	-182	gas
Propane	C_3H_8	-42	-188	gas
Butane	C_4H_{10}	0	-138	gas
Pentane	C_5H_{12}	36	-130	0.626 (liquid)
Hexane	C_6H_{14}	69	-95	0.659 (liquid)
Heptane	C_7H_{16}	98	-91	0.684 (liquid)
Octane	C_8H_{18}	126	-57	0.703 (liquid)
Nonage	C_9H_{20}	151	-54	0.718 (liquid)
Decane	$C_{10}H_{22}$	174	-30	0.730 (liquid)
Undecane	$C_{11}H_{24}$	196	-26	0.740 (liquid)
Dodecane	$C_{12}H_{26}$	216	-10	0.749 (liquid)
Hexadecane	$C_{16}H_{34}$	287	18	0.769 (liquid)
Icosane	$C_{20}H_{42}$	343	37	solid
Triacontane	$C_{30}H_{62}$	450	66	solid
Tetracontane	$C_{40}H_{82}$	525	82	solid
Pentacontane	$C_{50}H_{102}$	575	91	solid

[Osokogwn, 1(3): May., 2012]
ISSN: 2277-9655

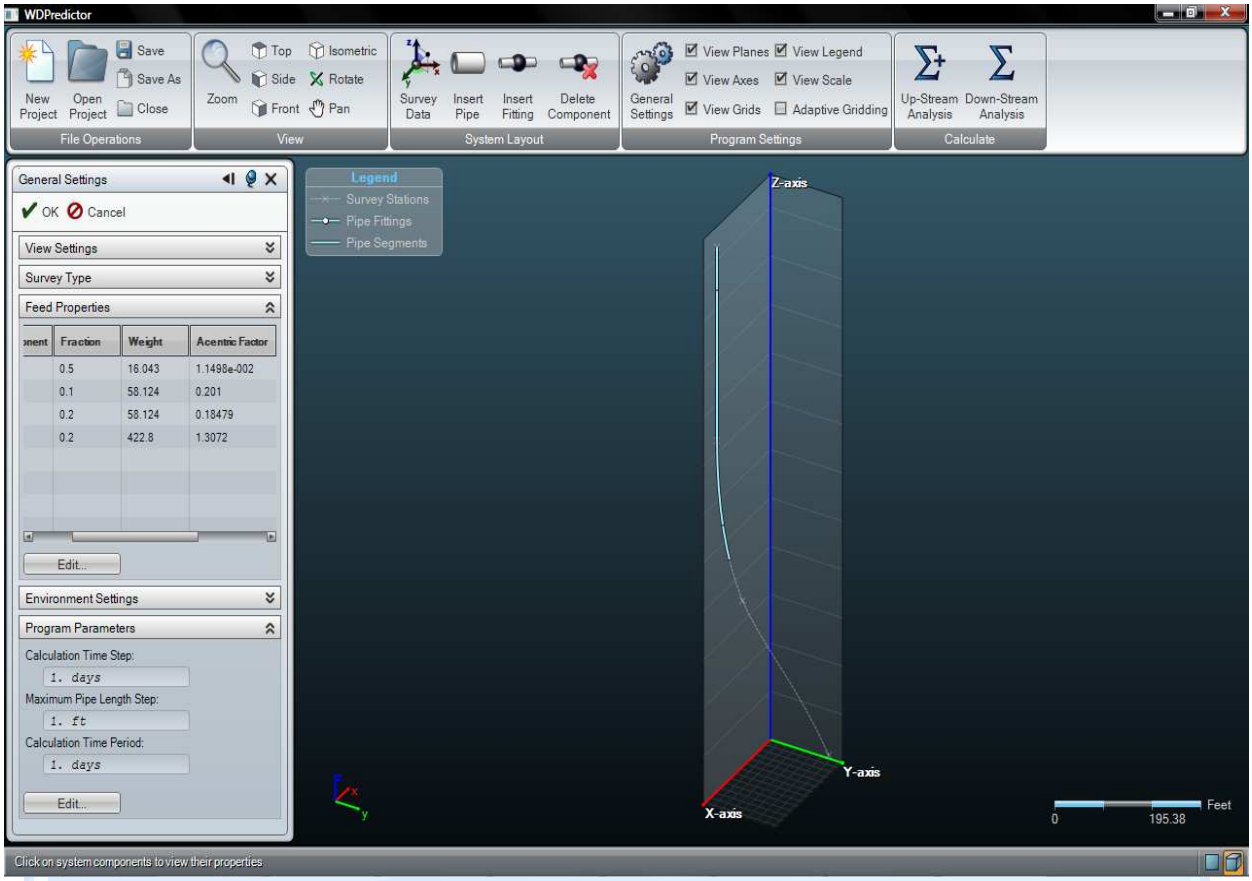

Figure A.5: WD-Predictor Environment showing Tubing as in segments